Journal of Renewable Materials
DOI:10.32604/jrm.2020.012136
Article

Tech Science Press

Mechanical Properties of Lime-Fly Ash-Sulphate Aluminum Cement Stabilized Loess

Liang Jia, Chunxiang Li and Jian Guo*

College of Civil Engineering, Lanzhou University of Technology, Lanzhou, 730050, China
*Correspondence Author: Jian Guo. Email: guojianlut@163.com
Received: 16 June 2020; Accepted: 10 August 2020

Abstract: Lime-fly ash stabilized loess has a poor early strength, which results in a later traffic opening time when it is used as road-base materials. Consideration of the significant early strength characteristics of sulphate aluminum cement (SAC), it is always added into the lime-fly ash mixtures to improve the early strength of stabilized loess. However, there is a scarcity of research on the mechanical behavior of lime-fly ash-SAC stabilized loess and there is a lack of quantitative evaluation of loess stabilized with binder materials. This research explored the effects of the amount of binder materials, curing time and porosity on the unconfined compressive strength (*UCS*), splitting tensile strength (*STS*), cohesion (c) and friction angle (φ) of lime-fly ash-SAC stabilized loess by a series of unconfined compressive tests (UCT) and splitting tensile tests (STT). The results indicate that an increase in curing time and a decrease in porosity lead to a continuous increase in the *UCS* and *STS* for lime-fly ash-SAC stabilized loess. The addition of SAC has a prominent enhancement in the early strength of lime-fly ash-SAC stabilized loess. When the curing time, porosity, and binder content were constant, the *UCS* and *STS* increase with increasing SAC content; For a stabilized loess with 30% binder content and 5% SAC content after 1 day of curing, the *UCS* was greater than 0.7 MPa, which meets the requirement of opening traffic, so lime-fly ash-SAC stabilized loess could be used as an excellent maintenance material for road-base; In accordance with the analysis of testing data, empirical relationships between the *UCS* and *STS* of lime-fly-SAC stabilized loess and key effect factors (binder materials content, curing time and porosity) were developed, which can provide references for reasonably selecting the amount of binder materials, compaction degree and curing period to meet the required strength of practical engineering. Finally, based on the Mohr-Coulomb theory and the above empirical relationships, a simpler method for calculating the c and φ of stabilized loess was proposed, with which, the shear strength parameters can be determined only by UCT or STT.

Keywords: Loess; sulphate aluminum cement; unconfined compressive strength; splitting tensile strength

1 Introduction

In China, loess occupies 6.6% of the territory and is chiefly distributed in arid and semi-arid regions [1–3]. In the natural state, loess has high strength and good stability, but deformation and the significant reduction of bearing capacity will occur when it is soaked with water [4,5]. When loess is fully immersed in water, the internal structure is destroyed, and significant additional deformation will occur under the action of self-weight stress or additional stresses. This phenomenon is called the collapsibility of loess [6]. The collapse of loess can cause engineering failures such as a landslide or huge foundation settlement, which pose a serious threat to people's lives and property [7]. Given this, various stabilizing measures were proposed by researchers to improve the strength and stability of loess [8–11].

The addition of lime, fly ash, cement, slag, lignin sulfonate, fiber and nanomaterials can significantly enhance the performance of fine-grained soils [12–17]. In the road construction, taking soils on site and stabilizing it with the above materials not only can meet the required quality but also save engineering costs. Adding lime to loess is a common method for improving the strength and stability of loess due to its low cost, simple mixing process and fine stabilizing effect [18]. Lime, loess and carbon dioxide from the air can react to form cementitious binder to increase the strength of loess [18]. However, the high plasticity index of loess causes a large temperature shrinkage and dry shrinkage of the lime stabilized loess [19]. Considering the promotion of sustainable development, attention has been paid to the utilization of industrial by-product. Moreover, lime-industrial waste (fly ash, slag, coal gangue) stabilized loess has high strength, good stability and small shrinkage potential [20]. In view of the low cost, high long-term strength and great stability of lime-fly ash stabilized loess, it is widely applied as road base materials in the loess region [2,21]. However, the application of lime-fly ash stabilized loess in the maintenance of subgrade and pavement requires a long-term traffic closure due to poor early strength, which greatly restricts the use of lime-fly ash stabilized loess in rapid maintenance projects of pavement. The addition of ordinary Portland cement in lime-fly ash stabilized loess can improve the early strength to some extent, but opening traffic requires at least 7 days of curing, which is not desirable [22,23].

In recent years, the application of sulphate aluminum cement (SAC) has attracted widespread attention from researchers and industry [24]. Generally, SAC presents similar properties to ordinary Portland cement in many aspects, such as controllable volume stability, outstanding anti-corrosive quality and good long-term strength [24]. In the production process of ordinary Portland cement, the raw calcium carbonate is ground and burned at a temperature of 1,450°C to form cement compounds. During this process, both the burning of fossil fuels and the calcination of calcium carbonate release large amounts of carbon dioxide, which poses a series of environmental problems [25]. However, the production of SAC only requires a calcination temperature of 1,250°C, which means less consumption of fossil fuel and the emission of carbon dioxide [26]. Besides, SAC has the characteristics of rapid hardening high early strength, great bonding strength and good environmental adaptability, and thus has been widely applied in rapid maintenance projects [27–29]. In order to reduce the amount of SAC to save the cost, SAC is always mixed with other binders such as lime and industrial waste residue in soil improvements [30–32]. In practical projects of soil reinforcement, it is necessary to determine the required binder content prior to construction, and the compaction degree and curing period also play an important role in strength development. In view of this, Consoli et al. [13] suggested that the curing time, binder content, and void/binder ratio can be used as appropriate parameters to predict the strength of stabilized soils. Nevertheless, the application of SAC in road-base is scarce. Also, there is a lack of literature on the strength prediction and binder dosage calculation of lime-industrial waste residue-SAC stabilized loess in road engineering. Generally, the failure form of road-base falls into two types. One is the crushing failure caused by the load of upper vehicles due to the insufficient compressive strength of materials. The other is reflection cracks caused by the cracking of lower subgrade due to the insufficient tensile strength of materials

[33,34]. In view of this, the need for evaluating the compressive and tensile strength of pavement base materials ensures long-term quality of roads.

This study, lime, fly ash and SAC were comprehensively used to loess improvement. A series of UCT and STT were performed to explore the strength development of lime-fly ash-SAC stabilized loess as a road-base material. Moreover, the empirical relationships of *UCS* and *STS* against binder content, porosity and curing time were developed. Finally, on the basis of the Mohr-Coulomb theory and the above empirical relationships, a simpler method for calculating the c and φ of stabilized loess was established.

2 Experiments

2.1 Materials

The loess was collected from the bottom (about 10 m in depth) of a construction pit located in Lanzhou University of Technology. To reach a homogeneous state in its particle distribution, the loess was air-dried, crushed, and finally passed through a standard sieve with a 0.5 mm opening size. The specific gravity of the loess determined by the water pycnometer method [35] is 2.71, and the liquid limit and plastic limit measured according to the method specified in GB/T50123 [36] are 25.00% and 10.14%, respectively. According to the Chinese standard (GT/T50145-2007), the loess used is a low liquid limit clay (CL). Other physical properties were achieved by referring to the literature related to Lanzhou loess [37], as shown in Tab. 1. The slaked lime and fly ash used were purchased from Gongyi Chemical Products Co., Ltd. (Henan province, China) with a specific gravity of 2.49 and 2.28, respectively. The SAC used was sourced from Shanghai Tongda Co., Ltd. with a specific gravity of 3.15. The chemical compositions for the loess, lime, fly ash and SAC are listed in Tab. 2.

Table 1: Some physical properities of the loess

Property	Value
Liquid limit	25.00%
Plastic limit	10.14%
Plasticity index	14.86%
Soil classification	CL
Specific gravity	2.71
Maximum dry density	1.78 g/cm^3
Optimum moisture content	15%
Friction Angle	29.6°
Cohesion	13.8 kPa

Table 2: Chemical compositions of the materials

Compositions (%)	SiO_2	Al_2O_3	Fe_2O_3	CaO	Na_2O	K_2O	MgO	$Ca(OH)_2$	$CaCO_3$	SO_3	TiO_2
Loess	50	8~15	4~5	10	–	2	2~3	–	–	–	–
Fly ash	≤56.96	30	≤4.63	≤1.5	–	–	≤2.8	–	–	–	–
Lime	≤2	–	–	–	–	–	≤2	≥94	≤4		
SAC	5.4	42.6	1.6	35.9	1.4	1.5	1.0	–	–	8.5	2.1

2.2 Specimen Preparation

In general, to meet the required strength for road-base built with lime-fly ash-SAC stabilized loess, the selected binder content is 20–30% of the total mass of the stabilized loess, and the mass ratio of lime to fly ash is 1:2 [38]. To reduce experimental workload, the amount of binder was determined as 20% (class I) and 30% (class II), in which the selected amount of SAC was 1% (I-1and II-1), 3% (I-2 and II-2) and 5% (I-3 and II-3), and the specific mixing ratios are presented in Tab. 3. The optimum moisture content (OMC) and maximum dry density (MDD) of lime-fly ash-SAC stabilized loess with different mixing proportions were achieved by standard compaction test. To establish the relationships of *UCS* and *STS* against porosity, the specimens with three different densities (MDD, MDD-0.1and MDD-0.2) for each mixing proportion were prepared. The specimens of UCT and STT were prepared by static compression method in a 61.8 mm inner diameter by 125 mm high hollow cylindrical metal mold [9]. The procedure of the specimen preparation referred to the method presented in Chinese standard GB/T50123 [36], as follows. The required amount of lime-fly ash-SAC stabilized loess for a specimen was first calculated, and then the amount of lime, fly ash, SAC, loess and water for a specimen were determined and weighed in accordance with the predesigned mixing ratios. After the loess, lime and fly ash were stirred evenly, the water was then added and continued the mixing process. After the mixture was mixed thoroughly, it was stored in a sealed plastic bag for 24 hours. Then a predetermined amount of SAC was added to the mixture, which was mixed well again. After the above processes, the mixture was divided into 5 uniform parts, and poured into the mold successively and compacted. Finally, the prepared specimen was labeled and placed in a curing box at a temperature of 20 ± 2°C and relative humidity of 95%, for a predetermined curing period (1, 4, 7 and 28 days).

Table 3: The OMC and MDD for specimens with various mix rations

Category	Lime: Fly-Ash: CSA: Loess	Binder content (%)	L (%)	F (%)	SAC (%)	MDD (g/cm^3)	OMC (%)
I-1	6.33: 12.67: 1: 80	20	6.33	12.67	1	1.66	17.6
I-2	5.67: 11.33: 3: 80		5.67	11.33	3	1.67	17.7
I-3	5: 10: 5: 80		5	10	5	1.68	17.8
II-1	9.67: 19.33: 1: 70	30	9.67	19.33	1	1.6	18.1
II-2	9: 18: 3: 70		9	18	3	1.62	18.3
II-3	8.33: 16.57: 5: 70		8.33	16.57	5	1.64	18.7

Note: L is lime content, F is fly ash content, SAC is sulphate aluminum cement content. Binder content is the total content of the lime, fly ash and SAC in the mixture.

3 Testing Methods

3.1 Standards Compaction Test

The standard compaction test was carried out according to the method described in ASTM D698 [39]. More than 5 lime-fly ash-SAC stabilized loess samples with different moisture were prepared for each mixing ratio, in which, two ones had a moisture content greater than the OMC and two were less than the OMC. After compaction, two small pieces of soil taken from the center of the sample was dried in an oven to define the moisture. Finally, the relation curve of dry density and moisture content was drawn, from which the OMC and MDD can be determined.

3.2 Unconfined Compression Tests

The UCT was performed following the method given in ASTM C39 [40]. A strain-controlled loading machine with a maximum capacity of 50 kN was employed for the UCT, and a loading rate of

1.2 mm/min was adopted. The *UCS* was calculated according to Eq. (1). To get more reliable results, a total of three specimens for each mixing ratio were prepared and tested at the same density and curing age, and the average *UCS* (the deviation value between these three strengths and the mean strength should be less than 10%) of these three specimens was assumed as the final *UCS*.

$$UCS(\text{kPa}) = \frac{4P}{\pi d^2} \tag{1}$$

where P is the maximum load value during the loading process, and d is the diameter of the specimen and adopted 61.8 mm.

3.3 Splitting Tensile Tests

The STT was carried out conforming to ASTM C496 [41], and *STS* was determined in agreement with Eq. (2), and the adopted *STS* was defined in the same way as that of *UCS*.

$$STS(\text{kPa}) = 1000 \times \frac{2P}{\pi dh}(\sin 2\alpha - \frac{a}{d}) \tag{2}$$

where P is the maximum load value during the loading process. The thickness of the splitting knife (a) is 12.70 mm, and the height and diameter (h and d) of the specimen are 125 mm and 61.8 mm respectively, and the central angle (α) of the half-bar is 0.127 rad.

4 Results and Discussion

4.1 Standard Compaction Test

Fig. 1 presents the relation curves of the dry density (ρ_d) and water content (ω) of lime-fly ash-SAC stabilized loess with different mix ratios. It can be seen that with the increase of binder content, the OMC increases from 15.6% to 21.6%, while the MDD exhibits an opposite tendency ranging from 1.67 g/cm^3 to 1.5 g/cm^3. For a given binder content, both the OMC and MDD increase with the increase of the SAC content and the OMC and MDD of the stabilized loess with different mixing ratios are summarized in Tab. 2. It can be well perceived that the more binder content is added to loess, the more water is needed to reach the MDD. This can be explained as the dissociation of $Ca(OH)_2$ in lime to produce more Ca^{2+} ions for the cation exchange reaction, which requires more water consumption. Also, an increase in the mean specific surface area of the mixture caused by the addition of binder requires more amount of water to lubricate the matrix [42]. The drop of the MDD caused by increasing binder content can attribute to the production of cementitious compounds and the flocculation of soil particles. When binders are added to the loess, a certain amount of flocculation produced by cation exchange in the mixture induces the flocculation of inter-particles and reduction of the plasticity, and thus results in the extra effort required to compact the mixture [20]. Moreover, a lower mean specific gravity than the loess of binder can also play an important role causing the reduction of the MDD. The positive effect of SAC on the MDD can be explained as a higher specific gravity than loess for SAC [7].

4.2 Effect of Curing Time on UCS and STS

The *UCS* and *STS* of lime-fly ash-SAC stabilized loess with different curing ages are presented in Fig. 2. It can be observed that an increasing curing time results in approximately linear growth in *UCS* and *STS*. This growth form is different from that of lime-fly ash stabilized loess, and the later presents a slow-growing early strength and a relatively quick-growing later strength [7]. However, the high early strength and rapid hardening characteristics of SAC result in a rapid-growing early strength for the lime-fly ash-SAC stabilized loess, and thus the growth rates in the early and late stages are nearly the same for lime-fly ash-SAC stabilized loess. The *UCS* is greater than 0.7 MPa for the stabilized loess with 30% binder and 5%

SAC content after 1 day of curing, which meets the requirement of opening traffic [38]. Therefore, the lime-fly ash-SAC stabilized loess first proposed in this study can be used as a quick maintenance material for road-base in the loess region. Also, the application of lime-fly ash-SAC stabilized loess in the road-base maintenance projects of loess region can avoid the use of bituminous base and thus greatly reduces the costs.

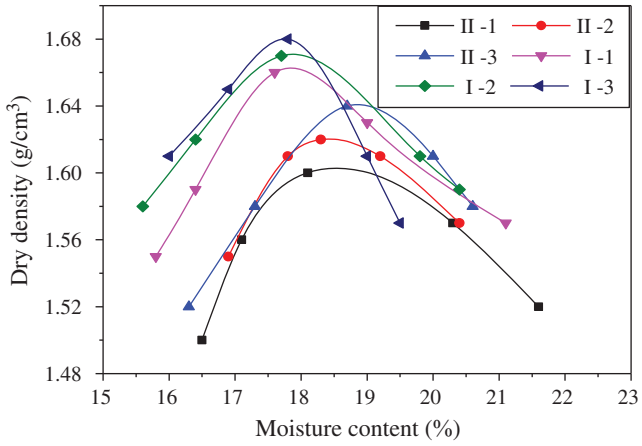

Figure 1: Compaction curves of lime-fly ash-SAC stabilized loess

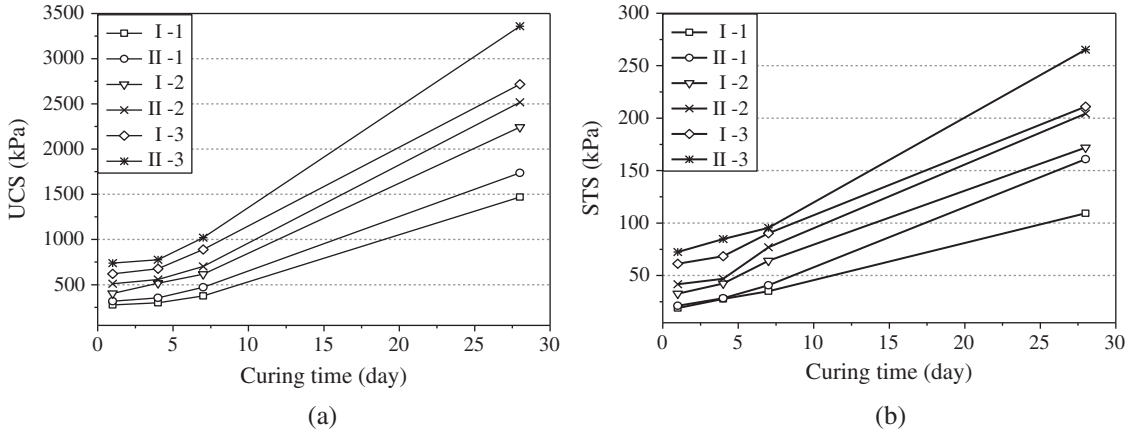

Figure 2: Variations of (a) *UCS* and (b) *STS* with curing time

The *UCS* with 7 days and 28 days of curing measured from this study and others are summarized in Tab. 4 [6,43–46], and it also can be observed more visually from Fig. 3 that the *UCS* of lime-fly ash-SAC stabilized loess with 30% binder content after 7 days of curing increases by 45% than that of lime stabilized loess, and increases by 64% after 28 days of curing. By comparing the *UCS* of loess stabilized with various binders such as cement, lime, nano-SiO_2 and fly ash, the *UCS* of lime-fly ash-SAC stabilized loess presents a greater growth rate, which indicated that SAC can enhance the early strength of stabilized loess more significantly than other binders.

4.3 Empirical Relationships between UCS and STS versus the Affecting Factors

According to the study performed by Consoli et al., the strength of stabilized soil increases with increasing volumetric binder content and decreases with increasing porosity (η), and a conclusion can be reached that an increase in the porosity of the stabilized soil can be partly counteracted by an increase in

volumetric binder content (L_V) to maintain the *STS* and *UCS* of stabilized soil at a definite value, thereby, η/L_V can play an important parameter to evaluate the strength of stabilized soil [13]. However, the variation trends of *UCS* (or *STS*) led by increasing volumetric binder content and decreasing porosity are strongly different, which makes the porosity/volumetric binder content ratio alone not a reasonable parameter to assess the *UCS* (or *STS*) [47]. For the above reason, the need to apply a power on one of the two variables (η and L_V) eliminates the difference mentioned above as far as possible. In this study, a power value of 0.12 was adopted to modify L_V. Moreover, according to Figs. 4 and 5, a slight change in SAC content induces a significant difference in the *UCS* (or *STS*) of lime-fly ash-SAC stabilized loess, that is, the existence of SAC produces a magnifying effect on the stabilizing potential of the binder materials (lime and fly ash). The main cause for the above magnifying effect is the existence of anhydrous calcium sulphoaluminate (C_4A_3S) and dicalcium silicate (C_2S) in SAC compared with ordinary portland cement. The C_4A_3S in SAC has a fast hydration process, during which, C_4A_3S can quickly react with gypsum ($CaSO_4.2H$) in cement to form ettringite (AFt) and also produce alumina gel (AH_3 gel). The C_2S in SAC forms hydrated calcium silicate gel (C-S-H gel) when it contacts with water, meanwhile, a certain amount of calcium hydroxide ($Ca(OH)_2$) is precipitated out. Subsequently, the secondary reaction will occur between the precipitated $Ca(OH)_2$, $CaSO_4.2H$ and AH_3 gel to produce AFt and single-sulfur calcium sulphoaluminate hydrate (AFm), which gives the mixture a higher density and thus enhances the strength [48].

Table 4: *UCS* of different stabilized loess (for 7 days and 28 days of curing)

References	Stabilized materials	Liquid limit (%)	Plastic limit (%)	7 days curing (MPa)	28 days curing (MPa)
Jia et al. [6]	Lime content: 23%	24.67	13.51	0.33	0.56
Zhang et al. [43]	Lime and fly ash: 30%	29.2	11.2	0.70	2.04
Chong et al. [44]	Cement content: 5%	23–25	15–16	0.79	1.32
	Cement content: 6%	23–25	15–16	0.88	2.51
Kong et al. [45]	Nano-SiO2: 2%	27.98	17.45	0.27	0.41
Phoak et al. [46]	Fly ash content: 30%	35.69	19.02	–	0.7
This study	Lime-fly ash-CSA(II-3)	25	10.14	1.02	3.36

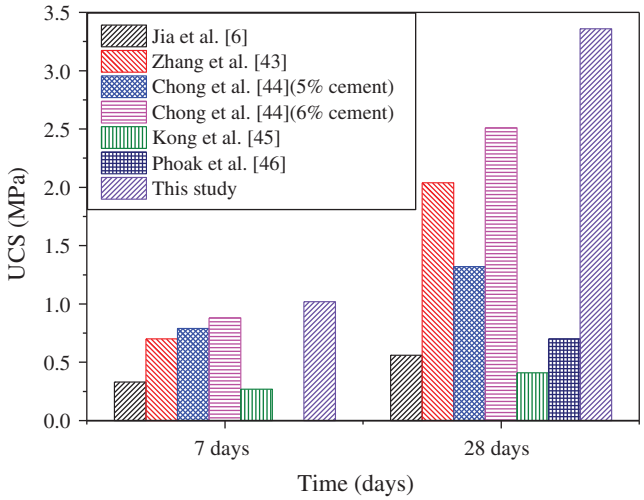

Figure 3: *UCS* of loess stabilized with different binders after 7 and 28 days of curing

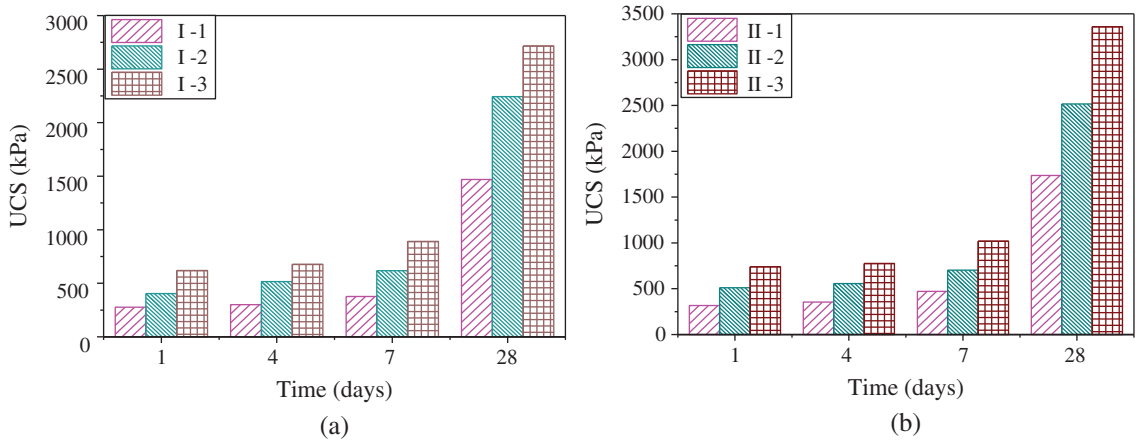

Figure 4: Effect of SAC content on the *UCS* of lime-fly ash-SAC stabilized loess with (a) 20% and (b) 30% binder content

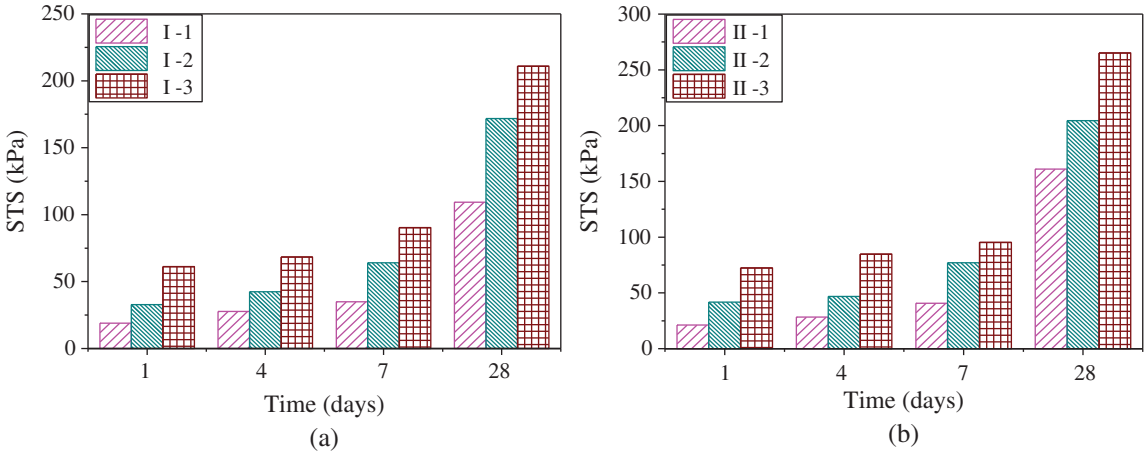

Figure 5: Effect of SAC content on the *STS* of lime-fly ash-SAC stabilized loess with (a) 20% and (b) 30% binder content

In summary, a reasonable functional form of *UCS* (or *STS*) against porosity (η), volumetric binder content (L_V) and volumetric SAC content (C_V) was first provided in this research, as presented in Eq. (3). The regression coefficients such as -0.52, 0.03 and 0.12 were obtained by trials and errors. Fig. 6 presents that the proposed function relationships of *UCS* versus η, L_V and C_V are in good agreement with the experimental data for lime-fly ash-SAC stabilized loess at 1, 4, 7 and 28 days of curing, and the coefficients of determination (R^2) are greater than 0.88. Furthermore, the proposed function relationship shows a good fit with the change trend of the measured *STS* for lime-fly ash-SAC stabilized loess at each curing age, as shown in Fig. 7, and the coefficients of determination (R^2) are greater than 0.85. The values of coefficient A in Eq. (3) are listed in Tab. 5. The η and L_V can be calculated by Eqs. (4) and (5) [49,50].

$$UCS \text{ or } STS = Ae^{-0.52\eta/C_V{}^{0.03}L_V{}^{0.12})} \tag{3}$$

$$\eta = 100 - \frac{100\left[\dfrac{v_s\rho_d\left(\dfrac{Lo}{100}\right)}{Gs_{Lo}} + \dfrac{v_s\rho_d\left(\dfrac{F}{100}\right)}{Gs_F} + \dfrac{v_s\rho_d\left(\dfrac{L}{100}\right)}{Gs_L} + \dfrac{v_s\rho_d\left(\dfrac{SAC}{100}\right)}{Gs_{SAC}}\right]}{V_S} \tag{4}$$

$$L_V = \frac{100\left[\dfrac{v_s\rho_d\left(\dfrac{F}{100}\right)}{Gs_F} + \dfrac{v_s\rho_d\left(\dfrac{L}{100}\right)}{Gs_L} + \dfrac{v_s\rho_d\left(\dfrac{SAC}{100}\right)}{Gs_{SAC}}\right]}{V_S} \tag{5}$$

where Lo is loess content and the specific gravity of the material used is as follows: loess $Gs_{Lo} = 2.71$, fly ash $G_{sF} = 2.89$, lime $G_{sL} = 2.49$, SAC $G_{sSAC} = 3.15$, and specimen volume $V_s = 375\ mm^3$.

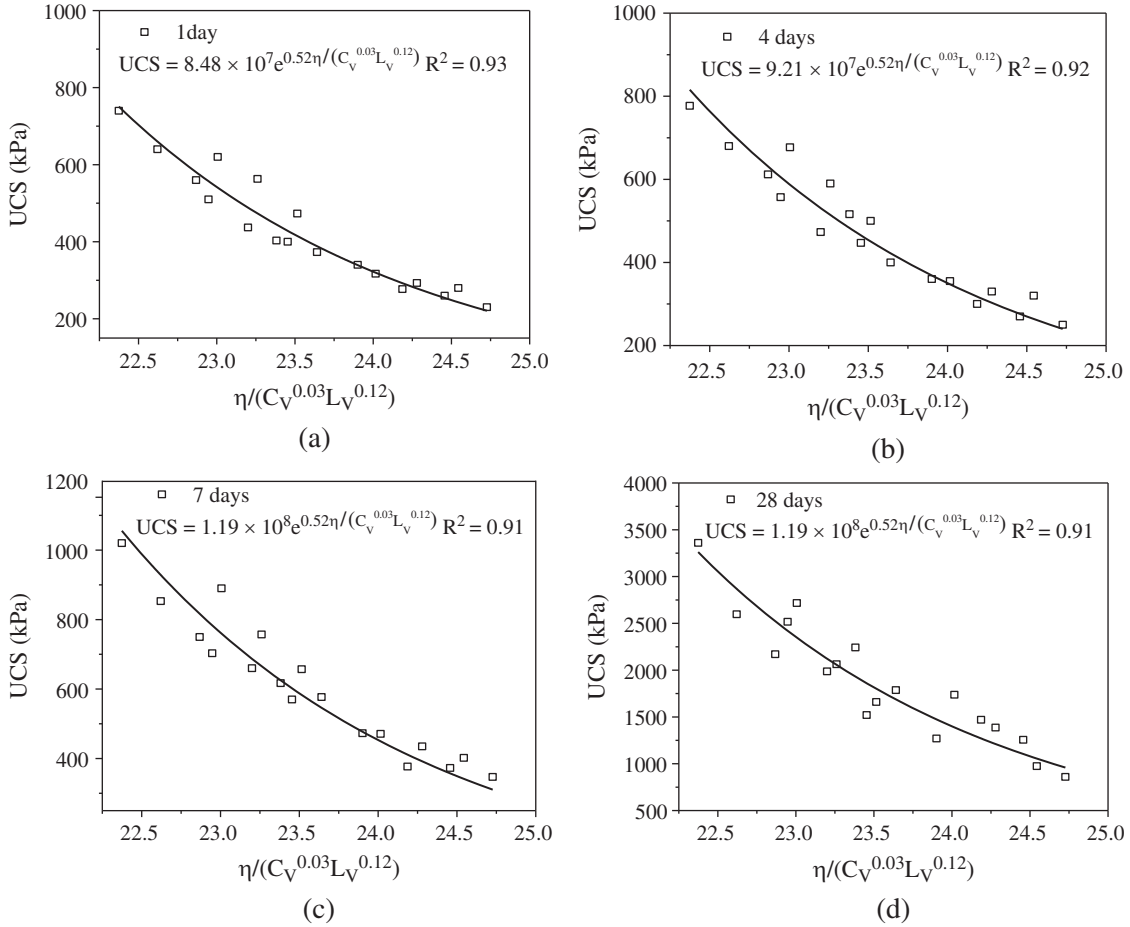

Figure 6: Variation of *UCS* with $\eta/(C_V{}^{0.03}L_V{}^{0.12})$ at different curing ages: (a) 1 day of curing, (b) 4 days of curing, (c) 7 days of curing, (d) 28 days of curing

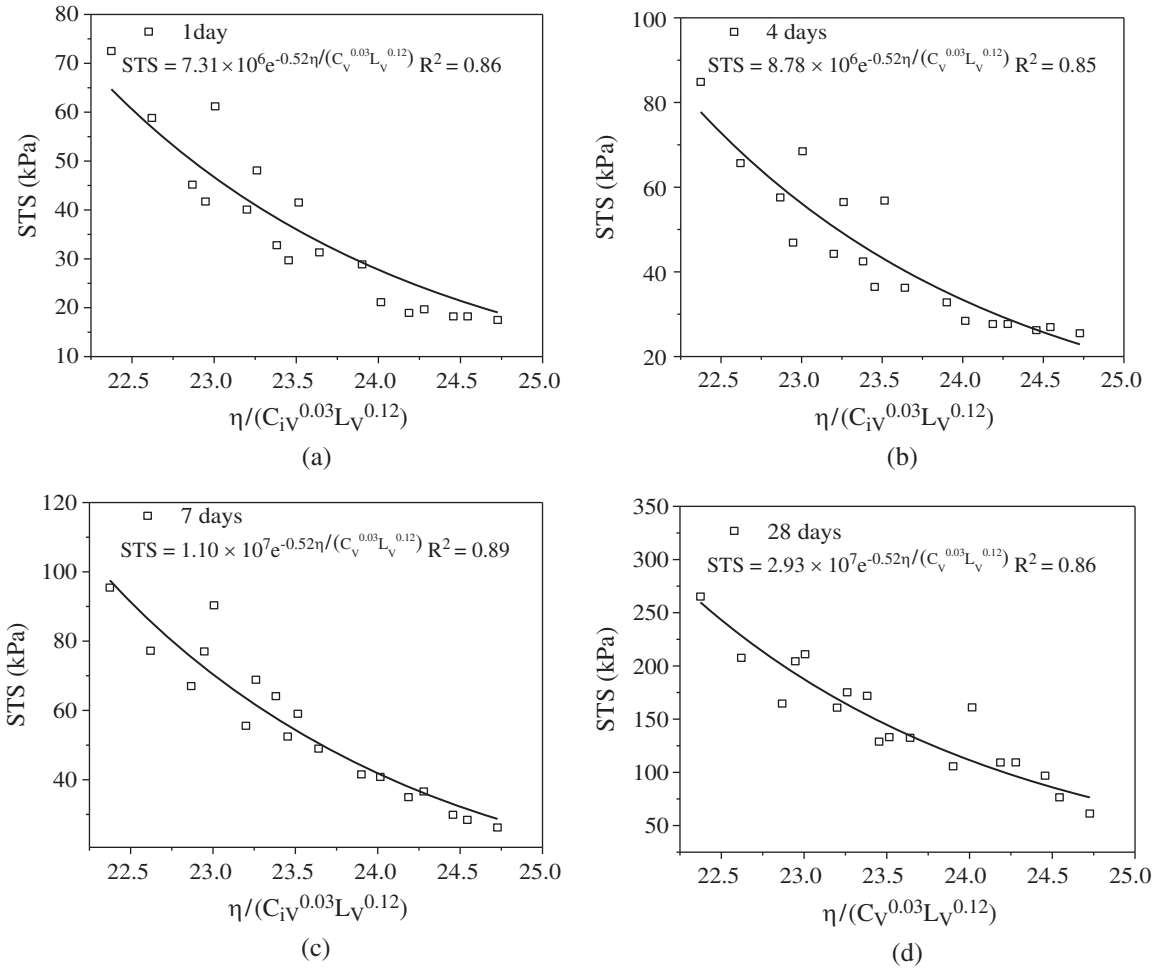

Figure 7: Variation of STS with $\eta/(C_V^{0.03}L_V^{0.12})$ at different curing ages: (a) 1 day of curing, (b) 4 days of curing, (c) 7 days of curing, (d) 28 days of curing

Table 5: coefficient *A* for *UCS* and *STS* of each curing time

Curing time (days)	*A*	
	UCS	*STS*
1	8.48 × 107	7.31 × 106
4	9.21 × 107	8.78 × 106
7	1.19 × 108	1.10 × 107
28	3.68 × 108	2.93 × 107

The observation of Tab. 5 indicates that the larger curing age *(t)*, the greater the value of *A* is for both *UCS* and *STS*. Fig. 8 displays the relationships of parameter *A* and *t*, which can be defined by applying an exponential function (Eq. (6)), and the value of *B* is 8.26×10^7 for predicting *UCS* and is 6.77×10^6 for predicting *STS*.

$$A=Be^{0.053t} \tag{6}$$

Combining Eqs. (3) and (6), a unique predicted function can be achieved linking the *UCS* (or *STS*) with η, L_V, C_V and t, as presented in Eqs. (7) and (8). A comparison was conducted for the measured and predicted *UCS* and *STS* based on Eqs. (7) and (8), as presented in Fig. 9. It can be readily observed that the predicted *UCS* and *STS* agree well with the measured ones for lime-fly ash-SAC stabilized loess. Therefore, Eqs. (7) and (8) are fairly reliable to predict the strength development for lime-fly ash-SAC stabilized loess. In actual projects, the engineer can adjust the compaction degree and the amount of binder or SAC according to the above methodology to meet the required strength and project schedule.

$$UCS = 8.26 \times 10^7 e^{0.053t-0.52\eta/C_V{}^{0.03}L_V{}^{0.12})} \tag{7}$$

$$STS = 6.77 \times 10^6 e^{0.053t-0.52\eta/C_V{}^{0.03}L_V{}^{0.12})} \tag{8}$$

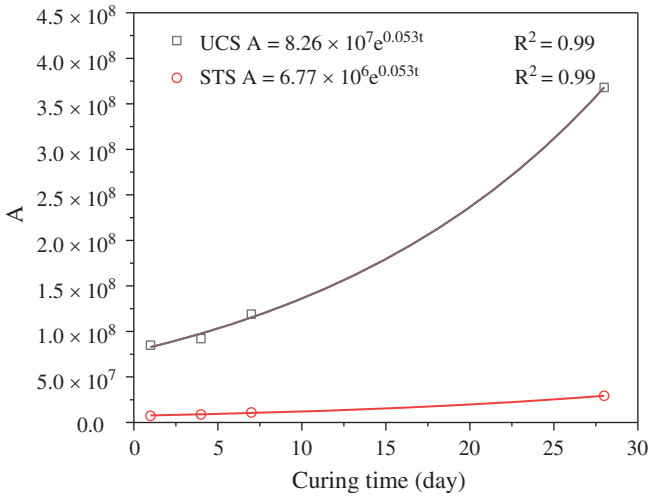

Figure 8: Correlation of A with t for UCS and STS

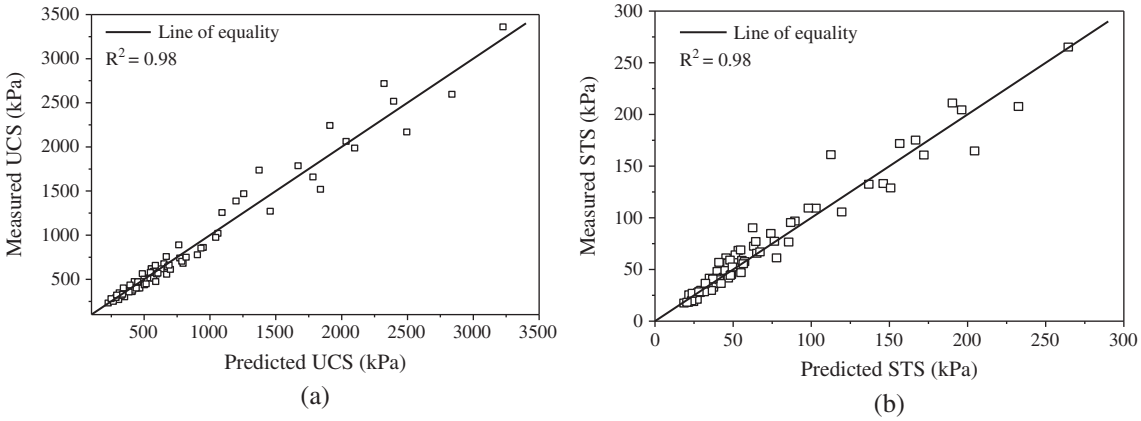

Figure 9: Comparison of predicted and measured strength for the lime-fly ash-SAC stabilized loess: (a) *UCS*; (b) *STS*

4.4 Parameters of Mohr–Coulomb Failure Envelope (c and φ)

4.4.1 Proposal of Method

For a given soil, friction angle (φ) and cohesion (c) are generally certain values, which keep the slope and intercept of Mohr–Coulomb failure envelope constant (Fig. 10), and thus result in the shear strength (τ) increasing linearly with the normal stress (σ), as shown in Eq. (9) [51].

$$\tau = c + \sigma \tan \varphi \tag{9}$$

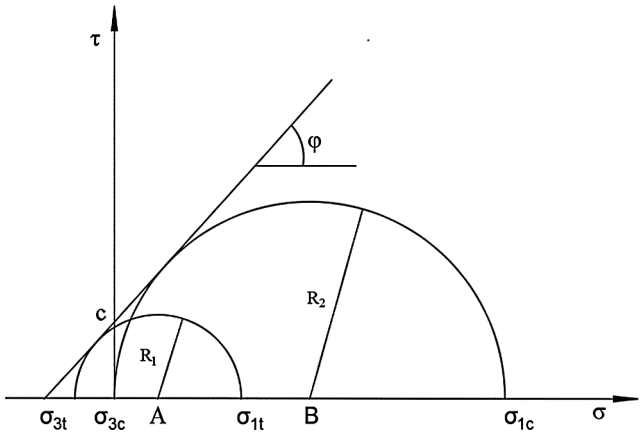

Figure 10: Mohr–Coulomb failure envelope and Mohr-circles based on the UCT and STT

In UCT and STT, the principal stress state of the specimen at failure is applied to analyze the relationships of *UCS* and *STS* versus φ and c, in which the maximum principal stress (σ_{1c}) and minimum principal stress (σ_{3c}) are $\sigma_{1c} = UCS$ and $\sigma_{3c} = 0$ for UCT, and $\sigma_{1t} = STS$ and $\sigma_{3t} = 3STS$ for STT [47].

The relationship between *UCS* and Mohr–Coulomb failure envelope parameters (φ and c) can be derived based on the geometric relationship shown in Fig. 10, as shown in Eq. (10).

$$\sin \varphi = \frac{UCS/2}{UCS/2 + c/\tan \varphi} \tag{10}$$

The relationship of *STS* against φ and c is shown in Eq. (11).

$$\sin \varphi = \frac{2STS}{STS + c/\tan \varphi} \tag{11}$$

The φ and c are calculated by simultaneously solving the Eqs. (10) and (11), and the results are presented in Eqs. (12) and (13), respectively.

$$\varphi = \arcsin\left(\frac{UCS - 4STS}{UCS - 2STS}\right) \tag{12}$$

$$c = \frac{UCS\left[1 - \left(\frac{UCS - 4STS}{UCS - 2STS}\right)\right]}{2\cos\left[\arcsin\left(\frac{UCS - 4STS}{UCS - 2STS}\right)\right]} \tag{13}$$

Previous studies have shown that the ratio of *STS* to *UCS* for stabilized soil is a constant [13,51] and can be written as $\zeta = STS/UCS$. Substituting ζ into Eqs. (12) and (13) obtains follows.

$$\varphi = \arcsin\left(\frac{1-4\zeta}{1-2\zeta}\right) \tag{14}$$

$$c = \frac{UCS\left[1-\left(\frac{1-4\zeta}{1-2\zeta}\right)\right]}{2\cos\left[\arcsin\left(\frac{1-4\zeta}{1-2\zeta}\right)\right]} \tag{15}$$

It can be seen from Eq. (14) that φ is also a constant and is not affected by porosity, binder content and curing time [47]. c is the function of ζ and *UCS*, while *UCS* is the function of η, L_V, C_V and t [47]. Therefore, c is the function of ζ, η, L_V, C_V and t.

4.4.2 The Application of the Proposed Method in Lime-Fly Ash-SAC Stabilized Loess

It can be obtained from Eqs. (7) and (8) that $\zeta = STS/UCS = 0.082$. Substituting ζ into Eq. (14), the φ of lime-fly ash-SAC stabilized loess can be obtained as given in Eq. (16).

$$\varphi = \arcsin\left(\frac{1-4\zeta}{1-2\zeta}\right) = \arcsin\left(\frac{1-4\times 0.082}{1-2\times 0.082}\right) = 53.4^{\circ} \tag{16}$$

As mentioned above, Brown holds that the φ of stabilized soil is between 40° and 60° [52]. In this research, the φ of lime-fly ash-SAC stabilized loess is in consistence with this conclusion, which proves the feasibility of the proposed method. Similarly, the c is achieved by substituting $\zeta = 0.082$ into Eq. (15), as given in Eq. (17).

$$c = 0.1652UCS \tag{17}$$

The above results show that friction angle does not change with the curing time, density and binder content of lime-fly ash-SAC stabilized loess. However, the cohesion of lime-fly ash-SAC stabilized loess changes with the above factors. Based on the unconfined compression test, the cohesion of lime-fly ash-SAC stabilized loess can be calculated by using Eq. (17). The relationships between c and φ versus *UCS* and *STS* are derived based on the Mohr-Coulomb theory and have been verified by Consoli et al. [13,51,53]. The prediction relationships for *UCS* and *STS* proposed in this study have been verified, as presented in Fig. 9. Consequently, the methodology proposed herein is an efficient alternative to the triaxial test, by which the cohesion of stabilized loess can be determined without the necessity of carrying out time-consuming triaxial tests.

5 Conclusions

In this paper, UCT and STT were carried out on lime-fly ash-SAC stabilized loess with different curing time, mixing ratio and density, and the method for calculating the friction angle and cohesion of the stabilized loess was also proposed based on the Mohr–Coulomb theory. The main conclusions can be drawn.

With an increase in binder content, the MDD increases from 1.5 to 1.67 g/cm^3, while the OMC drops from 21.6% to 15.6% for the lime-fly ash-SAC-loess mixture. For a given binder content, both the OMC and MDD increase with the increase of SAC content. The above phenomenon can be as the results of the increasing cation exchange reaction and some changes in the physical properties of the mixture, such as plasticity, specific gravity and specific surface area.

The *UCS* and *STS* of lime-fly ash-SAC stabilized loess increase approximately linearly with curing period. The addition of SAC in stabilized loess has a significant effect on the development of the early strength compared with loess stabilized with other inorganic binders, which can be attributed to the existence of anhydrous calcium sulphoaluminate (C_4A_3S) and dicalcium silicate (C_2S) in SAC accelerating the hydration reaction. It is worth noting that the stabilized loess with 30% binder content and 5% SAC content after 1 day of curing can meet the requirement of opening traffic, so it can be used as a rapid-maintenance material for road-base in the loess region.

The addition of binder generates a gain in both *UCS* and *STS* while increasing porosity causes a negative effect on the growth of *UCS* and *STS*. The ratio of η to L_V is not a reliable parameter to assess *UCS* and *STS* due to the difference between the effects of decreasing porosity and increasing binder content on *UCS* and *STS*, so modification was performed on η/L_V by applying a power on L_V. Meanwhile, the amount of SAC and curing age also play an important role in the development of *UCS* and *STS*. Finally, the prediction relationships of *UCS* and *STS* versus the four influencing factors were established, which have potential benefits for the safety assessment of loess improvement for road-base.

The relationships between Mohr–Coulomb failure envelope parameters (c and η) and *UCS* or *STS* were derived based on the Mohr–Coulomb theory and the researches by other scholars. The ratio of *STS* to *UCS* (ζ) is a constant ($\zeta = 0.082$), thereby, φ is independent of the curing age, binder content and porosity of lime-fly ash-SAC stabilized loess, while the change of c is related to *UCS* or *STS*. After a series of analysis and calculations, a simpler method for calculating c and φ of lime-fly ash-SAC stabilized loess was proposed, with which, the parameters of Mohr–Coulomb failure envelope can be determined only by the UCT or STT.

Acknowledgement: This study was supported by China Municipal Engineering Northwest Design and Research Institute Co. LTD, National Natural Science Foundation of China and the first-class subjects of Lanzhou University of Technology. The authors gratefully thank for their assistance.

Funding Statement: This study was funded by the National Natural Science Foundation of China (Grant Number 51568044), the first-class subjects of Lanzhou University of Technology (Grant Number 25-225209) and Research project of China Municipal Engineering Northwest Design and Research Institute Co. Ltd. (Grant Number XBSZKY2031).

Conflicts of Interest: The authors declare that they have no conflicts of interest to report regarding the present study.

References

1. Muhs, D., Cattle, S. R., Crouvi, O., Rousseau, D. D., Marcelo A. Zárate. (2014). Loess Records. *Mineral Dust: A key player in the Earth System*.
2. Liu, Z., Cai, C. S., Liu, F., Fan, F. (2016). Feasibility study of loess stabilization with fly ash-based geopolymer. *Journal of Materials in Civil Engineering, 28(5),* 10.
3. Li, P., Vanapalli, S. K., Li, T. (2016). Review of collapse triggering mechanism of collapsible soils due to wetting. *Journal of Rock Mechanics and Geotechnical Engineering, 8(2),* 256–274. DOI 10.1016/j.jrmge.2015.12.002.
4. Xie, W. L., Li, P., Zhang, M., Cheng, T., Wang, Y. (2018). Collapse behavior and microstructural evolution of loess soils from the loess plateau of China. *Journal of Mountain Science, 15(8),* 1642–1657. DOI 10.1007/s11629-018-5006-2.
5. Yuan, Z. X., Wang, L. M. (2009). Collapsibility and seismic settlement of loess. *Engineering Geology, 105(1–2),* 119–123. DOI 10.1016/j.enggeo.2008.12.002.
6. Zhang, F., Wang, G., Kamai, T., Chen, W., Zhang, D. et al. (2013). Undrained shear behavior of loess saturated with different concentrations of sodium chloride solution. *Engineering Geology, 155,* 69–79. DOI 10.1016/j.enggeo.2012.12.018.
7. Zhang, Y., Ye, W., Wang, Z. (2017). Study on the compaction effect factors of lime-treated loess highway embankments. *Civil Engineering Journal, 3(11),* 1008–1019. DOI 10.28991/cej-030933.

8. Jia, L., Guo, J., Zhou, Z., Fu, Y., Yao, K. (2019). Experimental investigation on strength development of lime stabilized loess. *RSC Advances, 9(34),* 19680–19689. DOI 10.1039/C9RA01914F.
9. Jia, L., Zhang, L., Guo, J., Yao, K., Lim, S. M. et al. (2019). Evaluation on strength properties of lime-slag stabilized loess as pavement base material. *Sustainability, 11(15),* 4099. DOI 10.3390/su11154099.
10. Yao, K., Chen, Q., Ho, J., Xiao, H., Lee, F. H. (2018). Strain-dependent shear stiffness of cement-treated marine clay. *Journal of Materials in Civil Engineering, 30(10),* 04018255. DOI 10.1061/(ASCE)MT.1943-5533.0002460.
11. Yao, K., Chen, Q., Xiao, H., Liu, Y., Lee, F. H. (2020). Small-strain shear modulus of cement-treated marine clay. *Journal of Materials in Civil Engineering, 32(6),* 04020114. DOI 10.1061/(ASCE)MT.1943-5533.0003153.
12. Behnood, A. (2018). Soil and clay stabilization with calcium- and non-calcium-based additives: a state-of-the-art review of challenges, approaches and techniques. *Transportation Geotechnics, 17,* 14–32. DOI 10.1016/j.trgeo.2018.08.002.
13. Consoli, N. C., De Moraes, R. R., Festugato, L. (2013). Parameters controlling tensile and compressive strength of fiber-reinforced cemented soil. *Journal of Materials in Civil Engineering, 25(10),* 1568–1573. DOI 10.1061/(ASCE)MT.1943-5533.0000555.
14. Yao, K., Wang, W., Li, N., Zhang, C., Wang, L. (2019). Investigation on strength and microstructure characteristics of nano-MgO admixed with cemented soft soil. *Construction and Building Materials, 206,* 160–168. DOI 10.1016/j.conbuildmat.2019.01.221.
15. Yao, K., Xiao, H., Chen, D., Liu, Y. (2019). A direct assessment for the stiffness development of artificially cemented clay. *Geotechnique, 69(8),* 741–747. DOI 10.1680/jgeot.18.T.010.
16. Yao, K., Pan, Y., Jia, L., Yi, J. T., Hu, J. et al. (2019). Strength evaluation of marine clay stabilized by cementitious binder. *Marine Georesources & Geotechnology, 38(6),* 1–14.
17. Wang, W., Li, Y., Yao, K., Li, N., Zhou, A. et al. (2019). Strength properties of nano-MgO and cement stabilized coastal silty clay subjected to sulfuric acid attack. *Marine Georesources & Geotechnology, 4,* 1–10.
18. Gao, Y., Qian, H., Li, X., Chen, J., Jia, H. (2018). Effects of lime treatment on the hydraulic conductivity and microstructure of loess. *Environmental Earth Sciences, 77(14),* 1–15. DOI 10.1007/s12665-018-7715-9.
19. Ma, F., Yang, J., Bai, X. (2017). Water sensitivity and microstructure of compacted loess. *Transportation Geotechnics, 11,* 41–56. DOI 10.1016/j.trgeo.2017.03.003.
20. Liu, Z., Cai, C. S., Liu, F., Fan, F. (2016). Feasibility study of loess stabilization with fly ash-based geopolymer. *Journal of Materials in Civil Engineering, 28(5),* 04016003. DOI 10.1061/(ASCE)MT.1943-5533.0001490.
21. Zhang, F., Pei, X., Yan, X. (2018). Physicochemical and mechanical properties of lime-treated loess. *Geotechnical and Geological Engineering, 36(1),* 685–696. DOI 10.1007/s10706-017-0341-6.
22. Kaniraj, S. R., Havanagi, V. G. (1999). Compressive strength of cement stabilized fly ash-soil mixtures. *Cement and Concrete Research, 29(5),* 673–677.
23. Neupane, K., Sriravindrarajah, R., Baweja, D., Chalmers, D. (2015). Effect of curing on the compressive strength development in structural grades of geocement concrete. *Construction and Building Materials, 94,* 241–248. DOI 10.1016/j.conbuildmat.2015.07.005.
24. Subramanian, S., Moon, S., Moon, J., Ku, T. (2018). CSA-treated sand for geotechnical application: microstructure analysis and rapid strength development. *Journal of Materials in Civil Engineering, 30(12),* 04018313. DOI 10.1061/(ASCE)MT.1943-5533.0002523.
25. Damtoft, J. S., Lukasik, J., Herfort, D., Sorrentino, D., Gartner, E. M. (2008). Sustainable development and climate change initiatives. *Cement and Concrete Research, 38(2),* 115–127. DOI 10.1016/j.cemconres.2007.09.008.
26. Juenger, M. C. G., Winnefeld, F., Provis, J. L., Ideker, J. H. (2011). Advances in alternative cementitious binders. *Cement and Concrete Research, 41(12),* 1232–1243. DOI 10.1016/j.cemconres.2010.11.012.
27. Cangiano, S., Meda, A., Plizzari, G. (2009). Rapid hardening concrete for the construction of a small span bridge. *Construction and Building Materials, 23(3),* 1329–1337. DOI 10.1016/j.conbuildmat.2008.07.030.
28. Subramanian, S., Moon, S. W., Moon, J., Ku, T. (2018). CSA-treated sand for geotechnical application: microstructure analysis and rapid strength development. *Journal of Materials in Civil Engineering, 30(12),* 04018313. DOI 10.1061/(ASCE)MT.1943-5533.0002523.

29. Frantzis, P. (2006). Effect of early-age temperature rise on the stability of rapid-hardening cement fiber composites. *Journal of Materials in Civil Engineering, 18(4),* 568–575. DOI 10.1061/(ASCE)0899-1561(2006)18:4(568).
30. Martin, L. H. J., Winnefeld, F., Muller, C. J., Lothenbach, B. (2015). Contribution of limestone to the hydration of calcium sulfoaluminate cement. *Cement and Concrete Composites, 62,* 204–211. DOI 10.1016/j.cemconcomp.2015.07.005.
31. Cangiano, S., Meda, A., Plizzari, G. (2000). Properties of blended sulfoaluminate belite cement. *Construction and Building Materials, 14(8),* 433–437. DOI 10.1016/S0950-0618(00)00050-7.
32. Garciamate, M., La Torre, A. G., Leonreina, L., Aranda, M. A., Santacruz, I. (2013). Hydration studies of calcium sulfoaluminate cements blended with fly ash. *Cement and Concrete Research, 54,* 12–20. DOI 10.1016/j.cemconres.2013.07.010.
33. Consoli, N. C., Rosa, F. D., Fonini, A. (2009). Plate load tests on cemented soil layers overlaying weaker soil. *Journal of Geotechnical and Geoenvironmental Engineering, 135(12),* 1846–1856. DOI 10.1061/(ASCE)GT.1943-5606.0000158.
34. Consoli, N. C., Thome, A., Donato, M., Graham, J. (2008). Loading tests on compacted soil, bottom-ash and lime layers. *Geotechnical Engineering, 161(1),* 29–38.
35. Saride, S., Rayabharapu, V. K., Vedpathak, S. (2015). Evaluation of rutting behaviour of geocell reinforced sand subgrades under repeated loading. *Indian Geotechnical Journal, 45(4),* 378–388. DOI 10.1007/s40098-014-0120-8.
36. GB/T50123 (1999). *Standard for soil test method*. China: Ministry of Construction.
37. Lv, Q., Wang, S., Wang, D., Wu, Z. (2014). Water stability mechanism of silicification grouted loess. *Bulletin of Engineering Geology and the Environment, 73(4),* 1025–1035. DOI 10.1007/s10064-014-0646-0.
38. JTG E51-2009 (2009). Test methods of materials stabilized with inorganic binders for highway engineering, China: Ministry of Transport of the People's China.
39. ASTM D698 (2012). *Standard test methods for laboratory compaction characteristics of soil using standard effort [12400ft-lbf/ft3 (600 kN-m/m3)]*. West Conshohocken, PA: ASTM International (ASTM), 13.
40. ASTM C39 (2012). *Standard test method for compressive strength of cylindrical concrete specimens*. West Conshohocken, PA: ASTM International (ASTM).
41. ASTM C496 (2011). *Standard test method for splitting tensile strength for brittle nuclear waste forms*. West Conshohocken, PA: ASTM International (ASTM).
42. Maneli, A., Kupolati, W. K., Abiola, O. S., Ndambuki, J. M. (2015). Influence of fly ash, ground-granulated blast furnace slag and lime on unconfined compressive strength of black cotton soil. *Road Materials and Pavement Design, 17(1),* 252–260. DOI 10.1080/14680629.2015.1066703.
43. Zhang, Y., Zhang, Z. (2013). Influence factor analysis on strength of lime-fly ash loess. *Engineering, 05(06),* 561–565. DOI 10.4236/eng.2013.56068.
44. Zhang, C. L., Jiang, G. L., Su, L. J., Zhou, G. D. (2017). Effect of cement on the stabilization of loess. *Journal of Mountain Science, 14(11),* 2325–2336. DOI 10.1007/s11629-017-4365-4.
45. Kong, R., Zhang, F. Y., Wang, G. H., Peng, J. B. (2018). Stabilization of loess using nano-sio2. *Materials, 11(6),* 1014. DOI 10.3390/ma11061014.
46. Phoak, S., Luo, Y. S., Li, S. N., Yin, Q. (2019). Influence of submergence on stabilization of loess in Shaanxi province by adding fly ash. *Applied Sciences-Basel, 9(1),* 68. DOI 10.3390/app9010068.
47. Consoli, N. C., da Silva Lopes, L. Jr., Heineck, K. S. (2009). Key parameters for the strength control of lime stabilized soils. *Journal of Materials in Civil Engineering, 21(5),* 210–216. DOI 10.1061/(ASCE)0899-1561(2009)21:5(210).
48. Wang, Y., Su, M. M. Z., Zhang, L. (2007). Classification of sulfoaluminate cement and the difference between its varieties. *China Cement, (02),* 52–56.
49. Consoli, N. C., Rocha, C. G., Silvani, C. (2014). Effect of curing temperature on the strength of sand, coal fly ash, and lime blends. *Journal of Materials in Civil Engineering, 26(8),* 06014015. DOI 10.1061/(ASCE)MT.1943-5533.0001011.

50. Merzouki, T., Bouasker, M., Khalifa, N. E., Mounanga, P. (2013). Contribution to the modeling of hydration and chemical shrinkage of slag-blended cement at early age. *Construction and Building Materials, 44,* 368–380. DOI 10.1016/j.conbuildmat.2013.02.022.
51. Consoli, N. C., Quinonez, R. A., Gonzalez, L. E., Lopez, R. A. (2014). A method proposed for the assessment of failure envelopes of cemented sandy soils. *Engineering Geology, 169,* 61–68. DOI 10.1016/j.enggeo.2013.11.016.
52. Brown, R. (2000). *Practical foundation engineering handbook*. 2nd. New York, NY: McGraw-Hill.
53. Consoli, N. C., Festugato, L., Consoli, B. S., Lopes, L. D. (2015). Assessing failure envelopes of soil-fly ash-lime blends. *Journal of Materials in Civil Engineering, 27(5),* 04014174. DOI 10.1061/(ASCE)MT.1943-5533.0001134.